JGR Space Physics

RESEARCH ARTICLE
10.1029/2020JA027899

Stochastic Evaluation of Pre-Earthquake TEC Enhancements

R. Ikuta[1], T. Hisada[1], G. Karakama[2], and O. Kuwano[3]

[1]Faculty of Science, Shizuoka University, Shizuoka, Japan, [2]Graduate School of Environmental Studies, Nagoya University, Nagoya, Japan, [3]JAMSTEC, Yokosuka, Japan

Key Points:
- Ionospheric TEC enhancement occurs so often without earthquakes, which can explain the "precursors" as just a product of chance
- A large TEC depletion spreading 500 km in diameter and lasting at least 120 min after the Tohoku-Oki earthquake
- Excluding window is in danger of mistaking the postseismic depletion for a preseismic enhancement

Supporting Information:
- Supporting Information S1
- Movie S1
- Movie S2
- Movie S3

Correspondence to:
R. Ikuta,
ikuta.ryoya@shizuoka.ac.jp

Citation:
Ikuta, R., Hisada, T., Karakama, G., & Kuwano, O. (2020). Stochastic evaluation of pre-earthquake TEC enhancements. *Journal of Geophysical Research: Space Physics*, *125*, e2020JA027899. https://doi.org/10.1029/2020JA027899

Received 21 FEB 2020
Accepted 16 OCT 2020
Accepted article online 24 OCT 2020

©2020. American Geophysical Union. All Rights Reserved.

Abstract Here we test the precursory enhancement in ionospheric total electron content (TEC) which has been reported by Heki (2011, https://doi.org/10.1029/2011GL047908) and numerous Global Navigation Satellite System (GNSS) TEC observational studies before the 2011 Mw9.0 Tohoku-Oki and many great earthquakes. We verify the frequency of this TEC enhancement via analysis of a 2-month vertical TEC (VTEC) time series that includes the Tohoku-Oki earthquake using the procedure, based on Akaike's information criterion, and threshold of Heki and Enomoto (2015, https://doi.org/10.1002/2015JA021353). The averaged occurrence rate of the TEC enhancement is much larger than that reported by Heki and Enomoto (2015, https://doi.org/10.1002/2015JA021353) when all of the visible GPS satellites at a given station are taken into account. The frequency assessment by Heki and Enomoto (2015, https://doi.org/10.1002/2015JA021353) using only one satellite underestimates the frequency of the TEC enhancement. In fact, the TEC enhancement is sufficiently frequent to explain all the reported enhancements prior to the great earthquakes as a product of chance. We also analyze the spatial distribution of the preseismic TEC enhancement and coseismic TEC depletion for the Tohoku-Oki earthquake with the data after reducing intertrace biases. We observe significant postseismic depletion that lasted at least 2 h after the earthquake and extended at least 500 km around the center of the large-slip area. This means that evaluation of the enhancements using reference curves which was adopted by Heki (2011, https://doi.org/10.1029/2011GL047908) and even by the recent papers (e.g., He & Heki 2016, https://doi.org/10.1002/2016GL069863; 2017, https://doi.org/10.1002/2017JA024012; 2018, https://doi.org/10.1029/2017JA024871) is in danger of mistaking a large and long-lasting postseismic TEC depletion for a preseismic enhancement.

1. Introduction

Precursory enhancement of the ionospheric total electron content (TEC) within a few tens of minutes before large earthquakes has been reported by Heki (2011) and numerous Global Navigation Satellite System (GNSS) TEC observational studies (e.g., He & Heki, 2016, 2017, 2018; Heki & Enomoto, 2013, 2015). Heki (2011) extracted the TEC enhancement prior to the 2011 Tohoku-Oki earthquake using a reference curve to model the slant TEC (STEC) time series, with the departure from the reference curve defining the TEC anomaly in the focal area. He excluded a 48-min time window surrounding the mainshock (from 34 min before to 14 min after the mainshock) from the STEC time series to deduce the reference curve and showed that the residual STEC began to increase 40 min before the earthquake, returning to the normal state when the postseismic acoustic wave reached the ionosphere (Heki, 2011). However, this approach has received criticism (e.g., Kamogawa & Kakinami, 2013; Masci et al., 2015). Kamogawa and Kakinami (2013) attributed the TEC enhancement reported by Heki (2011) to an artifact caused by the combined effects of TEC disturbances under active geomagnetic conditions and an ionospheric hole generated by a tsunami. Heki and Enomoto (2013) revisited the data to address this criticism and claimed that the tsunami did not make an ionospheric hole since their preseismic increase in the vertical TEC (VTEC) was comparable to the postseismic decrease. They suggested that the postseismic decrease was due to the recovery from the precursory TEC enhancement, rather than a post seismic tsunamigenic hole (Heki & Enomoto, 2013). This interpretation justifies the exclusion of the time window immediately surrounding the mainshock, for which the end time is generally set at 20 min after the mainshock, in deducing the reference VTEC curves in subsequent studies (e.g., He & Heki, 2016, 2017, 2018). However, He and Heki (2017) also considered the possibility of a postseismic hole when they studied the preseismic enhancement of Mw 7–8 earthquakes using the reference

curves. They claimed that the post seismic TEC depletions should be spatially limited above the focal area, even if they persist for a while, such that excluding the ±30-min time window surrounding the earthquake is enough to avoid these effects because the ionospheric penetration point (IPP) along the line of sight (LOS) between a station and satellite can pass through the area within this period (He & Heki, 2017). In addition to these rebuttals, Heki and Enomoto (2015) detected a positive break in the TEC time series (sudden increase in the TEC rate) without using reference curves before five great earthquakes based on Akaike's information criterion (AIC). They claimed that whether this positive break is space weather origin or not could be judged stochastically, even though the propagation of the positive break resembles a large-scale traveling ionospheric disturbance (LSTID) and there were active geomagnetic conditions during the period surrounding the 2011 Tohoku-Oki earthquake (Heki & Enomoto, 2015). They detected positive breaks for five of the eight analyzed Mw 8.2–9.2 earthquakes exceeding their TEC unit (TECU) threshold (3.0 TECU/h). They showed that the probability of the random occurrence of such breaks was below 1/10 per hour, which was the averaged frequency over the 3-week period surrounding the 2011 Tohoku-Oki earthquake. They then showed that the detection probability of such breaks during the 1.5-h period before the five earthquakes would be $(1.5 \times 1/10)^5$, which is too small to be considered a fortuity. However, their sampling approach would have underestimated the occurrence rate if the TEC enhancement varied between different satellites, since they used only one satellite to demonstrate the occurrence rate of the break.

Here we first test the occurrence rate of the TEC break using all of the visible satellites during a 61-day period surrounding the 2011 Tohoku-Oki earthquake. And then we also study the spatiotemporal characteristics of the TEC breaks. We then observe the post seismic VTEC depletion at the time of the Tohoku-Oki earthquake using data after reducing intertrace biases (ITBs), by which we study the potential risk in using the reference curve to estimate TEC enhancements.

2. TEC Data Processing

We calculated the VTEC time series from the L1 and L2 carrier phases of the Global Positioning System (GPS) signal for each GNSS station–satellite pair of the GNSS Earth Observation Network (GEONET) by implementing the following procedures.

2.1. Convert the Geometry-Free Linear Combination (L4) Into the TEC Deviation (ΔTEC)

We first obtained the phases of the L1 and L2 signals to calculate the carrier phase geometry-free combination (L4). We removed the cycle slips from L4 based on its jump and then shifted L4 to fit the geometry-free linear combination between the C1 and P2 codes to remove the phase ambiguities. This shifted L4 was multiplied by a constant $\frac{10^{-16} f_1^2 f_2^2}{40.308\left(f_1^2 - f_2^2\right)}$, where f_1 and f_2 are the dominant frequencies of the L1 and L2 signals, respectively, to obtain the TEC deviation (ΔTEC). ΔTEC is measured in TECU, where 1 TECU is equivalent to 10^{16} electrons m^{-2}, which also corresponds to 0.162 and 0.2675 m of the L1 and L2 signal delays, respectively.

The interfrequency biases (IFBs) of the stations and differential code biases (DCBs) of the satellites are both included in the ΔTEC data. We corrected for these biases to obtain meaningful slant TEC (STEC) values as follows:

$$STEC_{ij}(t) = \Delta TEC_{ij}(t) - DCB_j - IFB_i, \tag{1}$$

where t is the time and DCB_j and IFB_i correspond to the jth satellite and ith receiver, respectively. STEC was then converted to VTEC as follows:

$$VTEC_{ij}(t) = STEC_{ij}(t)\cos\psi_{ij}(t), \tag{2}$$

where ψ_{ij} is the incident angle of the signal which penetrates a thin ionosphere at IPP at 300 km above the ground.

The satellite's DCBs between C1 and P2 were calculated from the P1–C1 and P1–P2 code biases provided by the University of Bern (https://www.aiub.unibe.ch/). The receiver's IFBs between C1 and P2 were provided by the Electronic Navigation Research Institute (ENRI) (Sakai, 2005).

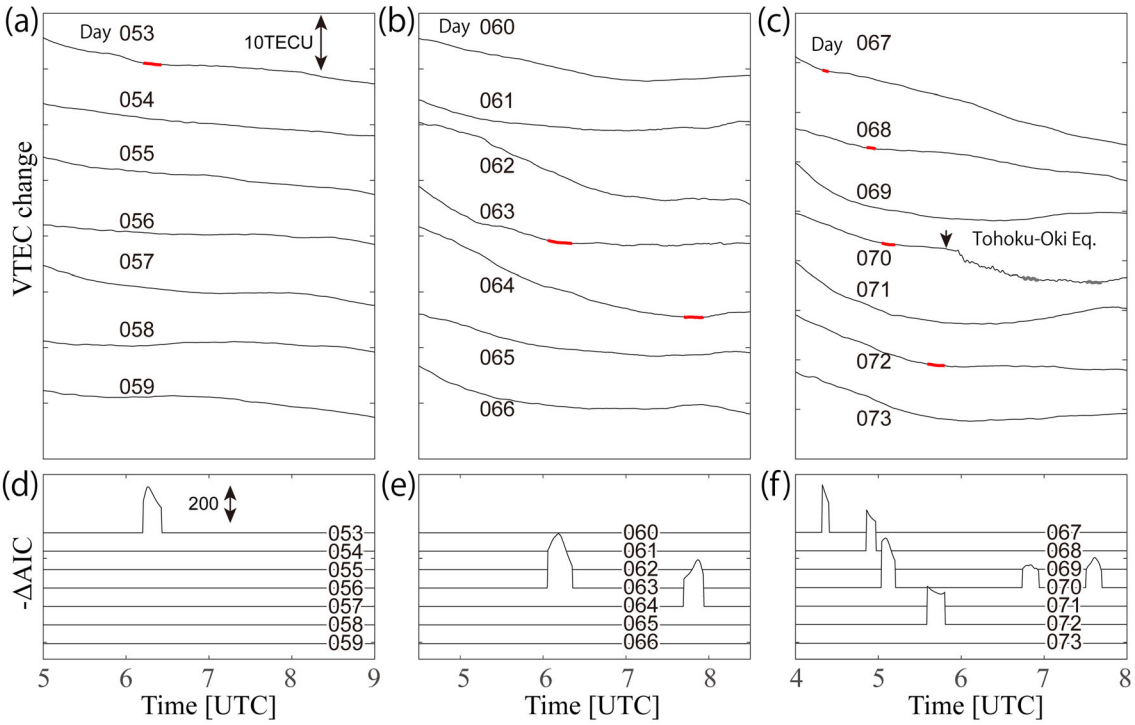

Figure 1. VTEC time series for the three-week period surrounding the 2011 Tohoku-Oki earthquake (same data set as used in making figure 6 of Heki and Enomoto (2015) for the same satellite (PRN15)–GNSS station (3009) pair. (a–c) VTEC time series. The red sections represent significant positive breaks (±30-min time window) that exceed 3 TECU/h and 75% of the original rate. The gray sections shortly after the Tohoku-Oki earthquake also represent positive breaks but not counted considering postseismic variation. (d–f) –ΔAIC calculated for (a)–(c), respectively.

2.2. TEC Break Detection

Heki and Enomoto (2015) evaluated the occurrence rate of the TEC enhancement in the VTEC time series using only one station–satellite pair; we follow their methodology here. A moving window was adopted that fits a pair of lines to the VTEC curve, with the break between the two lines set at the middle of the window. The significance of the break on the fit was determined by calculating the difference of AIC value between the two lines with break and a single line that was fit to the entire VTEC curve in the window. This difference was denoted as –ΔAIC; a pair of lines was judged to provide a better fit to the VTEC curve than a single line when –ΔAIC was positive. The TEC enhancement was then evaluated by comparing the increase in slope of the latter line to that of the former line when –ΔAIC was positive. The break was regarded as a "significant positive break" when the increase in slope between the two linear fits exceeded a certain threshold. Here we expand the approach of Heki and Enomoto (2015) by applying this procedure to all of the visible satellites from GNSS station 3009 instead of using only a single satellite–station pair. (They used only PRN15.) This approach is more reasonable to simulate the situation that a precursor seeker can choose any one of all visible satellites when they look for a positive break prior to a great earthquake. We adopt a ±30-min time window and regard an increase that is larger than 3.0 TECU/h (absolute) and 75% of the original rate (relative) as a significant positive break, following Heki and Enomoto (2015).

3. Results: Spatiotemporal Distribution of Positive Breaks

Figure 1 shows the VTEC time series for the 3-week period surrounding the 2011 Tohoku-Oki earthquake, using the same data set as Heki and Enomoto (2015) (satellite PRN15 and GNSS station 3009); the time series looks similar to that in figure 6 of Heki and Enomoto (2015). Positive breaks are detected seven times (red dots in Figure 1), including the preseismic break before the Tohoku-Oki earthquake, as observed by Heki and Enomoto (2015). The two breaks just after the Tohoku-Oki earthquake are not taken into account here (gray dots in Figure 1), as they were mentioned by Heki and Enomoto (2015).

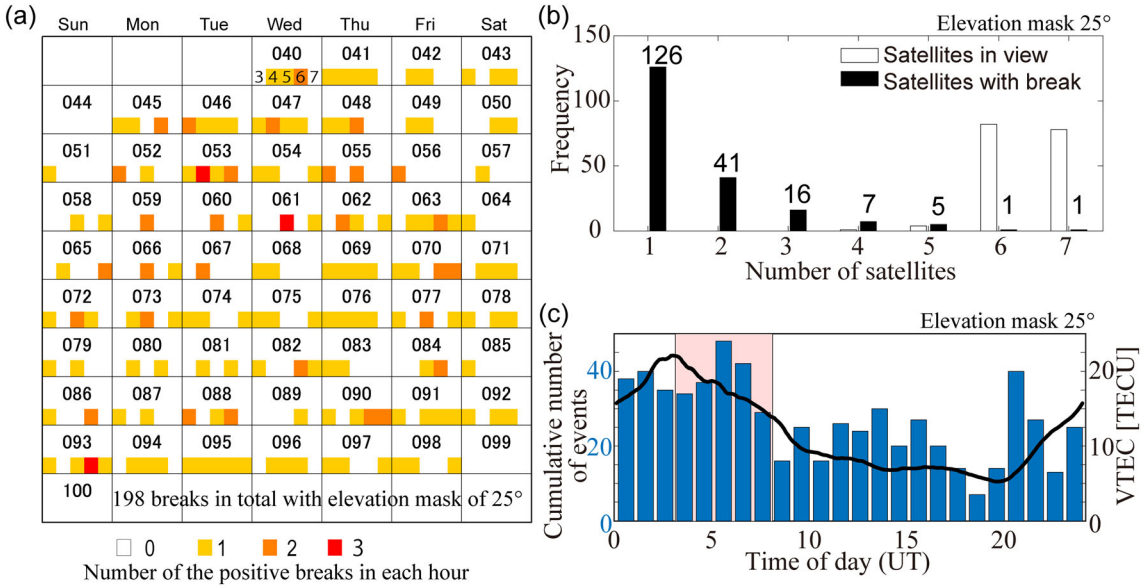

Figure 2. Frequency of positive TEC breaks during the 61-day period. (a) Number of positive breaks in calendar time, with an elevation mask angle of 25°. The number at the top of each cell is the day of year. The small numbers in the day 040 cell denote the five 1-h periods, which span from 03:00 to 08:00 UTC. The colors indicate the number of detected breaks in each 1-h period. (b) Frequency of satellites in view that detected a positive break, with an elevation mask angle of 25°. The white bars show the number of satellites in view when a positive break is detected. The black bars show the number of satellites that simultaneously detected a break. (c) Frequency of positive TEC breaks as a function of time of day during the 61-day period. The blue bars indicate the cumulative number of positive TEC break events that were detected during each hour. The solid line shows the 61-day-averaged VTEC time series. The shaded magenta region highlights the time of day that was the focus of the analysis in (a) and (b) (03:00–08:00 UTC).

We apply this analysis to the 61-day VTEC time series from 9 February (DOY40) to 10 April 2011 (DOY100). The positive break rate should have been accurately evaluated by Heki and Enomoto (2015) if it was simultaneously observed by all of the visible satellites. However, their positive break rate, which was evaluated using only one satellite, would be an underestimate if it was independently observed by each satellite because they would have missed positive breaks that occurred at satellites other than PRN15 at different times in the study period.

Figure 2a shows the number of detected significant positive breaks during the daytime (12:00–17:00 local time, LT; 03:00–08:00 UTC) for each day within the 61-day period. The breaks are calculated using all of the visible satellites with an elevation angle higher than 25°. If a period where the slope exceeds the threshold overlapped with a period from one or more other satellites, then these periods are regarded as one event. A total of 198 positive break events are detected within the 305-h observation period, resulting in an averaged occurrence rate of 0.65 times per hour. Approximately 36% of the breaks are detected simultaneously by multiple satellites, with the remaining 64% detected by one satellite (Figure 2b). The positive break 40 min before the Tohoku-Oki earthquake is detected by two satellites (PRN15 and 26) from the station 3009.

The diurnal variations in Figure 2c show that the occurrence rate of the positive break is higher in the daytime (09:00–17:00 LT; 00:00–08:00 UTC) and early morning (05:00–07:00 LT; 20:00–22:00 UTC). Positive breaks are detected about three times more frequently during the daytime than in the predawn hours (02:00–05:00 LT; 17:00–20:00 UTC), which is explained by variations in the background VTEC level. The high rate of break detection in the early morning is explained by TEC enhancement at dawn.

The positive break detection is also highly dependent on the LOS configuration. Figure 3a shows the spatial distribution of the detection rate of breaks at subionospheric points (SIPs), which is calculated by dividing the number of detected positive breaks by the SIP density. More positive breaks tend to be detected when the satellites are at a lower elevation angle. The detection rate is very high when the elevation is below 20°, especially in the southern sky. Figure 3b shows the relationship between the elevation mask and number of detected TEC breaks. The number of detected events is proportional to the number of satellites in view

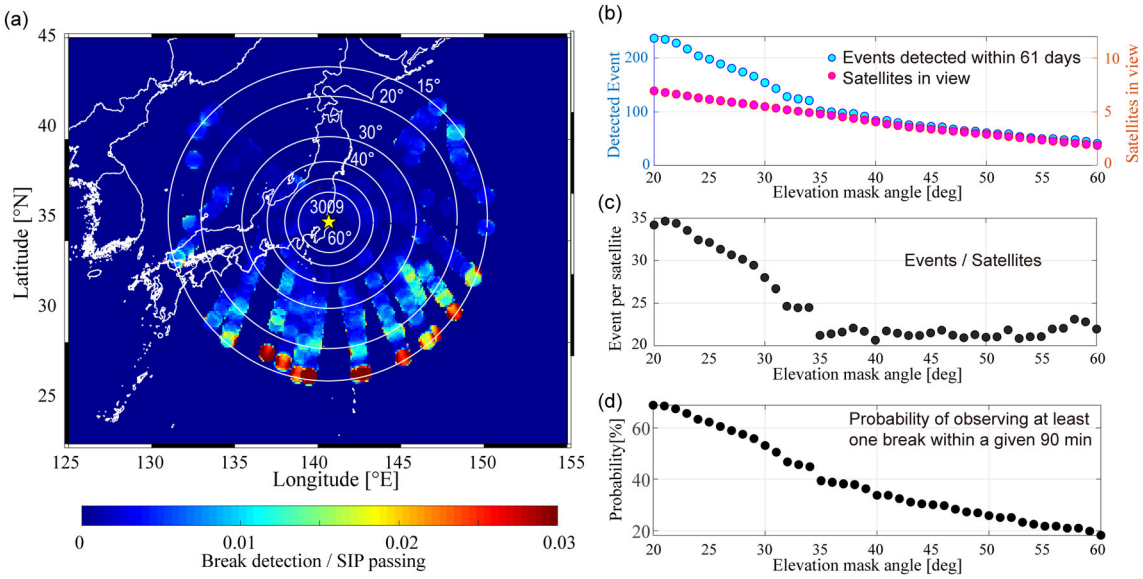

Figure 3. (a) Number of detected events and satellites in view against various elevation mask angles. (b) Number of events detected within the 61-day period (cyan) and average number of satellites in view (magenta) for a range of elevation mask angles. (c) Number of detected positive break events divided by the number of satellites in view. The expected number of events per satellite is approximately constant when the elevation mask angle is larger than 35°. (d) Probability of observing at least one break within a given 90 min assuming a Poisson process with different elevation mask angles.

when the elevation mask angle is larger than 35°. However, the number of detected events increases much more rapidly than the number of satellites in view when the elevation mask angle is less than 35°. This trend should be due to unstable VTEC behavior in the low-angle LOS, as in this case the ray paths travel longer distances through the ionosphere. When a 35° elevation mask angle is applied, a total of 102 positive TEC breaks are detected during the 61-day period (305 h). Each satellite detects an average of 21–22 breaks during the 61-day period with elevation mask angle of 35° (Figure 3c). This detection rate is similar to that in Heki and Enomoto (2015), where seven breaks were detected with satellite PRN15 over a 21-day period. Therefore, the occurrence rate of positive breaks considering all satellites in view is about five times larger than that Heki and Enomoto (2015) observed.

4. Discussion

The results of the stochastic TEC evaluation illustrate that the significant positive breaks are observed much more often than reported by Heki and Enomoto (2015). The average occurrence rate of the TEC positive breaks measured under the same conditions and threshold as those of Heki and Enomoto (2015), and the inclusion of all of the visible satellites, is 0.33 times per hour with a 35° elevation mask angle. This occurrence rate seems not enough low to rule out the possibility of product of chance for preseismic positive TEC breaks. Furthermore, considering that they adopted even lower elevation mask angles in detecting the preseismic enhancement for some earthquakes, the expected occurrence rate would be even higher than it.

Here we first evaluate the probability of the positive TEC breaks observed as just a product of chance before the five of eight great earthquakes reported by Heki and Enomoto (2015) considering the applied elevation mask angles. We then test some of the basis for precursor that Heki (2011) and his group have presented, based on the spatiotemporal VTEC distribution before and after the 2011 Tohoku-Oki earthquake.

4.1. Probability of the Preseismic Breaks

Heki and Enomoto (2015) reported significant positive TEC breaks (exceeding the absolute 3.0 TECU/h and relative 75% threshold) before five of eight Mw 8–9 earthquakes. We evaluate the probability of the case where the breaks are observed within 90 min before an earthquake assuming a Poisson process. The probability of observing n events during a time period, in which μ events are expected to occur on average, is expressed as follows:

$$f(n) = \frac{\mu^n}{n!} e^{-\mu}. \quad (3)$$

For example, when a 30° elevation mask angle is assumed, the average occurrence rate is 0.76 times per 90 min ($\mu = 0.76$) and the probability of observing at least one event during the time period is $1 - f(0) = 53\%$. Figure 3d shows the probability calculated for various elevation mask angles. With higher or lower elevation mask angles of 35° or 25°, the probability decreases or increases to 39% or 62%, respectively. The Heki and Enomoto (2015)'s 62% detection rate of the preseismic positive TEC breaks (five of the eight great earthquakes) corresponds to our estimated probability with 25° elevation mask angle even though the earthquake number of eight is too low to be evaluated stochastically. Regarding their actual elevation mask adopted to these earthquakes, they included breaks at very low elevation angles such as 15° for the 2012 Mw8.6 North Sumatra Earthquake. Then our 25° elevation mask angle is not too low to compare with their results. As a consequence, we cannot rule out a possibility that the detection of the positive TEC breaks before the five great earthquakes was not a precursor but a product of chance.

4.2. Correspondence Between the Preseismic and Post Seismic TEC Changes

We next test the correspondence between the preseismic and post seismic TEC changes reported by Heki and Enomoto (2013), where they proposed a temporal TEC variation model, with the postseismic drop representing a recovery from the preseismic increase (as opposed to a net decrease). We follow their analysis by testing the correlation between the preeismic increase and postseismic decrease in the VTEC time series around the source area. They modeled the VTEC time series from satellite PRN26 during the 3-h period surrounding the mainshock, which consisted of four lines connected by three breaks (Figure 4a; same as figure 3a in Heki and Enomoto (2013) but with the data analyzed using our procedure). They assumed that period A represented the background steady decrease in afternoon VTEC. Periods B and C correspond to the preseismic increase and coseismic decrease, respectively. They compared the integrated changes during B and C relative to the trend during A, and found that the increase in B was comparable to the decrease in C, which led them to report no net post seismic VTEC decrease (Heki & Enomoto, 2013). However, their analysis only incorporated seven GNSS stations that were approximately aligned. We extend the GNSS station coverage to test the spatial distribution of the VTEC changes. Figure 4b shows the relationship between the two quantities for the broad GNSS station distribution shown in the map. This result indicates that the coincidence between the increase and decrease is not universal across the region but rather limited to the stations selected by Heki and Enomoto (2013). The spatial distributions of the increase and the decrease during periods B and C, respectively, exhibit notably different patterns (Figures 4c and 4d).

This demonstration was prepared by Heki and Enomoto (2013) to respond to the criticism by Kamogawa and Kakinami (2013) that the preseismic increase should be an artifact as a result of the postseismic drop (tsunamigenic hole). Now a part of their rebuttal seems invalid, and we have to reconsider the possibility that the criticism by Kamogawa and Kakinami (2013) is reasonable.

4.3. Propagation of the TEC Enhancement

Heki and Enomoto (2013) has already pointed out that a LSTID, which traveled at ~0.3 km/s from north to south and arrived at the source area ~1 h before the mainshock, can provide one potential explanation for the TEC enhancement before the Tohoku-Oki earthquake. However, Heki and Enomoto (2015) showed that the appearance of the breaks within the latitude range of the ruptured fault area is simultaneous and then suggested that the signatures of the breaks differ from that due to space weather. Figure 5a shows the arrival time distribution of the TEC breaks for satellite PRN15. The break is represented by the –ΔAIC peak, which propagates from north to south, with a temporary acceleration seen around 04:50 UTC above the source region of the Tohoku-Oki earthquake. This acceleration corresponds to the reported simultaneous enhancement. However, these accelerations/decelerations often occur during LSTID propagation, such that the LSTID propagation is not necessarily constant in velocity and direction. Figures 5b and 5c and Movie S1 in the supporting information show the –ΔAIC propagation on the day of the Tohoku-Oki earthquake (DOY70) and the previous day (DOY69). The positive/negative breaks change the propagation velocity and frequently appear and disappear during the LSTID propagation, as their nature. For example, positive

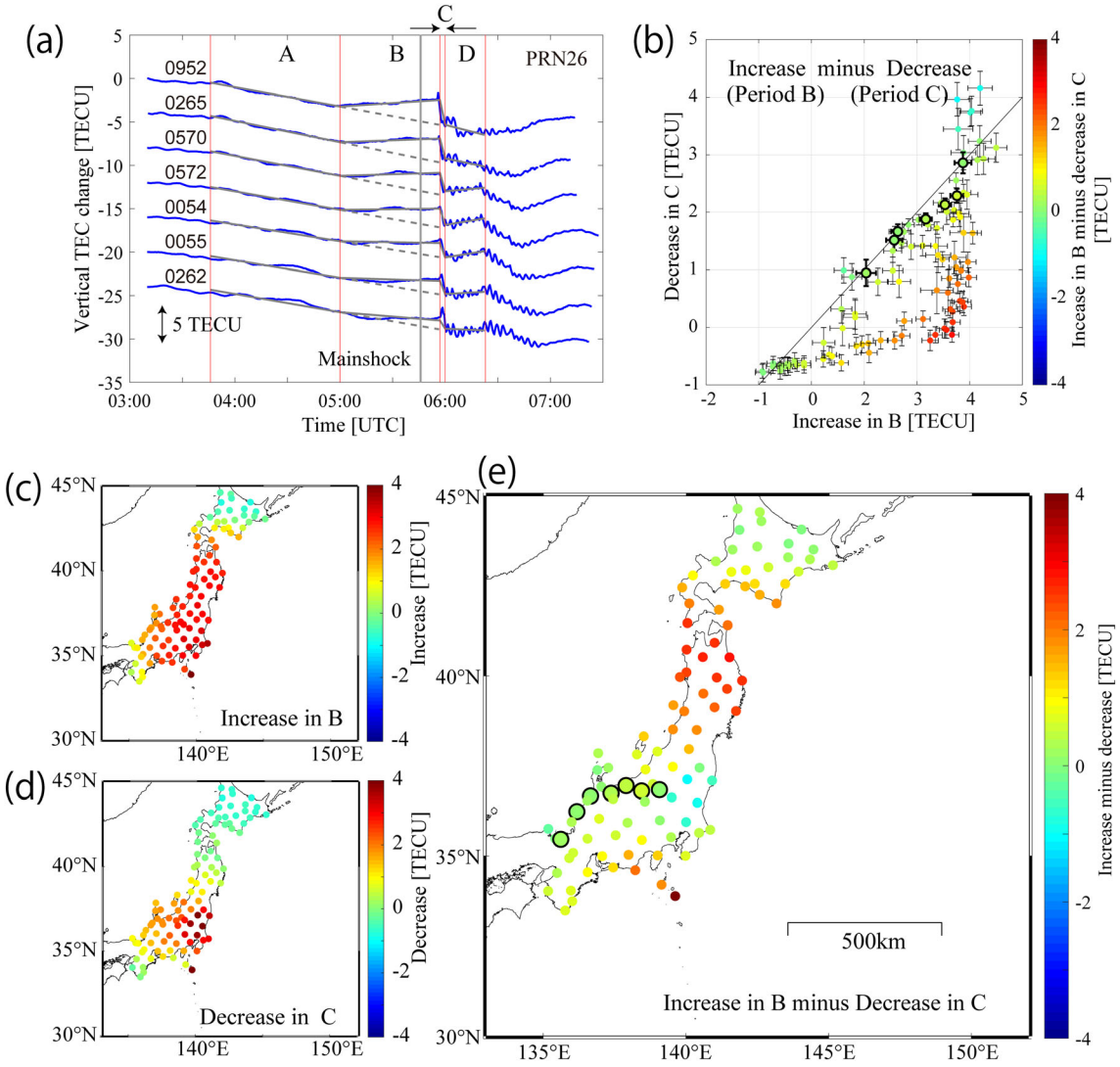

Figure 4. (a) VTEC time series from satellite PRN26 at seven GPS stations with various focal distances from the Tohoku-Oki earthquake epicenter. The ~3-h period surrounding the mainshock (marked by the vertical gray line), spanning from 03:45 UTC (2 h before the earthquake) to 06:25 UTC (~40 min after the earthquake), is divided into four segments (marked by the vertical red lines), which represent the (A) normal background, (B) precursory enhancement, (C) coseismic drop, and (D) postseismic periods, and a linear fit to each segment is determined (gray line segments). This figure is the same as figure 3a in Heki and Enomoto (2013), with the exception of the estimated VTEC time series used here. (b) Difference between the period B increase and period C decrease. The stations that were used by Heki and Enomoto (2013) are indicated by circles with thick lines. The error bars denote 1σ uncertainties. The observed difference is shown by the marker color. This figure is the same as figure 3c in Heki and Enomoto (2013), with the exception of the additional stations used in the analysis. (c) Spatial distribution of the degree of preseismic increase during period B at the stations. (d) Spatial distribution of the degree of postseismic decrease during period C at the stations. (e) Spatial distribution of the difference between the period B increase and period C decrease. The stations used by Heki and Enomoto (2013) are indicated by the larger circles with thick lines.

breaks appear simultaneously even on DOY69 (from 35 to 37°N around 05:40 UTC). This indicates that the acceleration of the positive TEC break is not a special phenomenon and also not significant as an evidence for its seismic origin.

4.4. Spatiotemporal Distribution of Post Seismic VTEC Depletion

A large post seismic TEC depletion was observed around the source region at the time of the Tohoku-Oki earthquake, as reported from observations (e.g., Kakinami et al., 2012; Kamogawa et al., 2016; Saito et al., 2011) and numerical models (Shinagawa et al., 2013). Here we analyze this postseismic depletion from a spatiotemporal perspective.

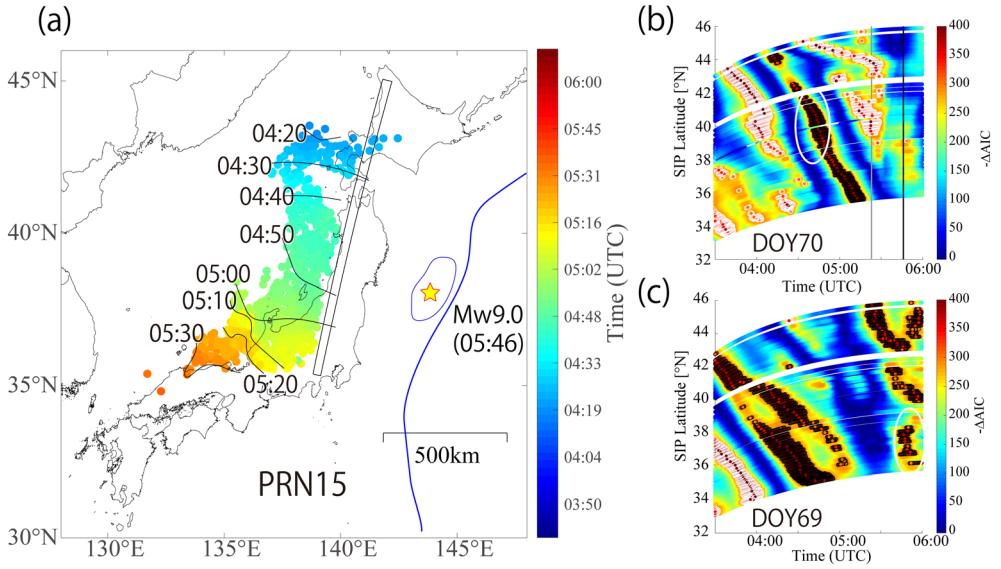

Figure 5. (a) Arrival time of the TEC break in the ±30-min window about the mainshock (05:46 UTC). The circles show the SIPs for satellite PRN15 at the time of the peak −ΔAIC value, whose slope is larger than the threshold (3.0 TECU/h and 75%), which represents the positive TEC break. The contours show the arrival time in 10-min intervals. The thick blue line marks the Japan Trench, and the star shows the epicenter of the 2011 Tohoku-Oki earthquake. The area enclosed by the thin blue line is the large-slip area (>10 m) that was determined by Ikuta et al. (2012). The rectangle extending from 35°N to 45°N shows the area of the selected stations that was used to depict the −ΔAIC propagation in Figures 5b and 5c. (b) −ΔAIC propagation among the selected stations for satellite PRN15 before the Tohoku-Oki earthquake (05:46 UTC on DOY70). The circles with black and white edges indicate the positive and negative breaks, respectively, for −ΔAIC values larger than 300. The vertical black line marks the time of the mainshock. The vertical gray line denotes 05:23 UTC, which corresponds the start of the 30-min window, which includes the coseismic disturbance (CID) starting at 05:53 UTC. The white ellipse around 04:40 UTC shows the acceleration of the LSTID propagation (a positive break), which Heki and Enomoto (2015) highlighted as a simultaneous appearance. (c) Same as Figure 5b but for the previous day (DOY69). The white ellipse around 05:40 UTC shows the acceleration of the LSTID propagation (a positive break).

We correct the ITBs due to the ambiguity of the code pseudo range, as mentioned in the Appendix, to observe the faint spatial variations in the VTEC time series. Figure 6 shows the spatial distribution of the corrected VTECs for satellite PRN26 and PRN15, whose SIPs pass through the large-slip area around the time of the mainshock. A round-shaped hole is seen around the epicenter, even 54 min after the earthquake with PRN26 (Figure 6b). The TEC values at the center of the depletion area are ~5 TECU less than those of the surrounding area. The PRN15 also shows significant TEC depletion after the mainshock around the source area (Figures 6d and 6e). The postseismic depletion can be seen more significantly in the movies. Movie S2 shows the preseismic and post seismic TEC variations at a 30-s sampling interval. The movie indicates that the first significant coseismic disturbance (CID) appears above the source area at 05:55 UTC for satellite PRN26, which is ~9 min after the mainshock. This CID propagation has been reported by many papers (e.g., Astafyeva et al., 2011; Kakinami et al., 2012; Tsugawa et al., 2011). At least four positive peaks, each with a different velocity, propagate from the source region to the southwest and to the north, with the amplitude of the first wave being especially large. A hole that is centered at the radiant point of the CID emerges at around 06:05 UTC, after these peaks propagated across the area. Four other satellites also show a postseismic hole, even though its outline is not as sharp as that observed with satellite PRN26 because their SIPs are not just above the large slip area at the moment of the mainshock (Movie S3). Movie S3 shows that postseismic VTEC depletion is observed, even 120 min after the mainshock, and extends at least 500 km around the high-slip area for all of the satellites in view (PRN9, 15, 12, and 27). The spatial extent of the depletion area is not necessarily isotropic but rather elongate in the northwest direction from the radiant point as described by Astafyeva et al. (2013), which may reflect the alignment of the lifted area along the trench.

He and Heki (2016) studied the three-dimensional distribution of the ionospheric anomalies prior to three large earthquakes in Chile (Mw8.2, 8.4, and 8.8). They modeled the VTEC curves with the polynomials of time with degrees 3–5, excluding the intervals from the onsets of the anomalies detected using AIC to

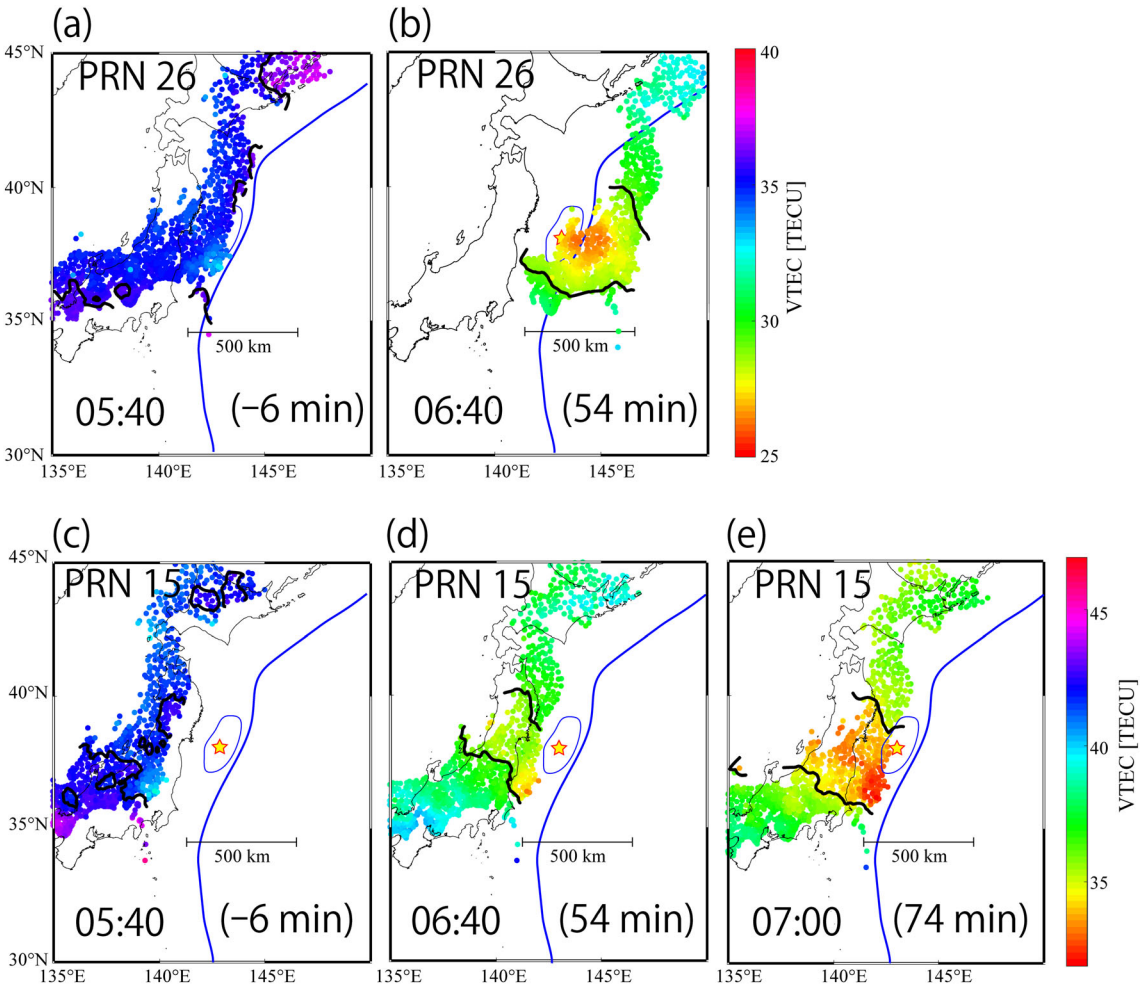

Figure 6. Absolute VTEC distribution with elevation mask angle of 20°. Satellite PRN26 at (a) 05:40 and (b) 06:40 UTC and satellite PRN15 at (c) 05:40, (d) 06:40, and (e) 07:00 UTC on 11 March 2011. The dots are color coded to show the absolute VTEC value for each IPP location at 300 km height. The thick black line shows the contour of the value 3 TECU larger than the lowest value for each time. The thick blue line shows the Japan Trench, and the red star shows the epicenter of the 2011 Tohoku-Oki earthquake. The area enclosed by the thin blue line is the large-slip area (>10 m) that was determined by Ikuta et al. (2012). The times in parentheses indicate the lapse times relative to the mainshock.

20 min after the earthquakes. However, the 20 min may be too short and their result is in danger of mistaking a large and long-lasting postseismic depletion for a preseismic enhancement. This should be also the case of He and Heki (2018) which conducted three-dimensional tomography of ionospheric anomaly before the 2015 Illapel earthquake. They calculated STEC residual using excluding window whose start was given by the −ΔAIC, and the ending time was assigned 25 min after the earthquake. He and Heki (2017) also studied the preseismic TEC enhancement before M 7–8 earthquakes using the reference curves and claimed that these depletions should be limited spatially above the focal area, even if postseismic holes exist, such that excluding the approximately ±30-min window around the earthquake is enough to avoid these effects since the IPP passes through the area within this period. However, they must have considered the temporal and spatial extent of the postseismic depletion more carefully when adopting the window of data to exclude. The spatial extent of the depleted area could be wider than their assumption. We should evaluate it with the actual data or at least numerical simulation like Shinagawa et al. (2013).

5. Conclusions

We stochastically evaluated the occurrence rate of the positive TEC breaks proposed by Heki and Enomoto (2015) using the same procedure and threshold as in their study. Our averaged occurrence rate

of TEC enhancement was much larger than that reported by Heki and Enomoto (2015) since we used all of the visible GPS satellites at GNSS station 3009. We detected 198 positive breaks within the 305-h time period using a 25° elevation mask angle. This corresponds to 62% probability that at least one positive break occurs within a given 90-min period assuming a Poisson process. This probability explains the fact that the TEC enhancement was observed in five out of eight huge earthquakes, which is much larger than the probability of $(1.5 \times 1/10)^5$ estimated by Heki and Enomoto (2015). Therefore, we cannot rule out the possibility that the preseismic VTEC changes, detected using the same procedure and threshold within 90 min before the 2011 Tohoku-Oki earthquake and the other four great earthquakes, are just a product of chance.

We also studied spatiotemporal characteristics of the TEC break to find that the positive/negative breaks often change the propagation velocity and even appear and disappear during the LSTID propagation as their nature. This suggests that the acceleration of the positive TEC break proposed by Heki and Enomoto (2015) is not a special phenomenon and also not significant as an evidence for its seismic origin.

We also analyzed the spatial distribution of the post seismic TEC depletion for the Tohoku-Oki earthquake with the data after reducing ITBs. A significant postseismic depletion that lasted at least 2 h after the earthquake and extended at least 500 km around the center of the large-slip area was observed. This means that evaluation of the enhancements using the reference curves with the short excluding time window which was adopted by Heki (2011) and even by the recent papers (e.g., He & Heki, 2016, 2017, 2018) is in danger of mistaking a large and long-lasting postseismic depletion for a preseismic enhancement. We cannot conclude that the TEC enhancements that Heki (2011) and the following papers have reported are not true precursors just by this observation of the Tohoku-Oki earthquake case and the stochastic evaluation. However, we cannot find any positive materials supporting their idea that the TEC enhancements are seismic origin.

Appendix A: Intertrace Bias (ITB) Correction

The TEC traces still show biases of up to a few TECU, even between adjacent stations, after correcting the DCBs and IFBs for the satellites and stations, respectively. An example of the VTEC distribution at a moment for PRN15 is shown in Figure A1a. A random variation up to a few TECU is seen in the residual distribution after the local spatial averages are subtracted from the VTEC. A pair of STEC traces with a common satellite will show almost constant bias during a period when the satellite is continuously visible. We recognize these biases as ITBs, which should arise from uncertainties in the code pseudo range. The pseudo range has large variances up to a few TECU, as well as a drift bias that cannot be fit very well by the L4 shift (as described in section 2.1), even though the pseudo range is free of integer ambiguity. We therefore need to

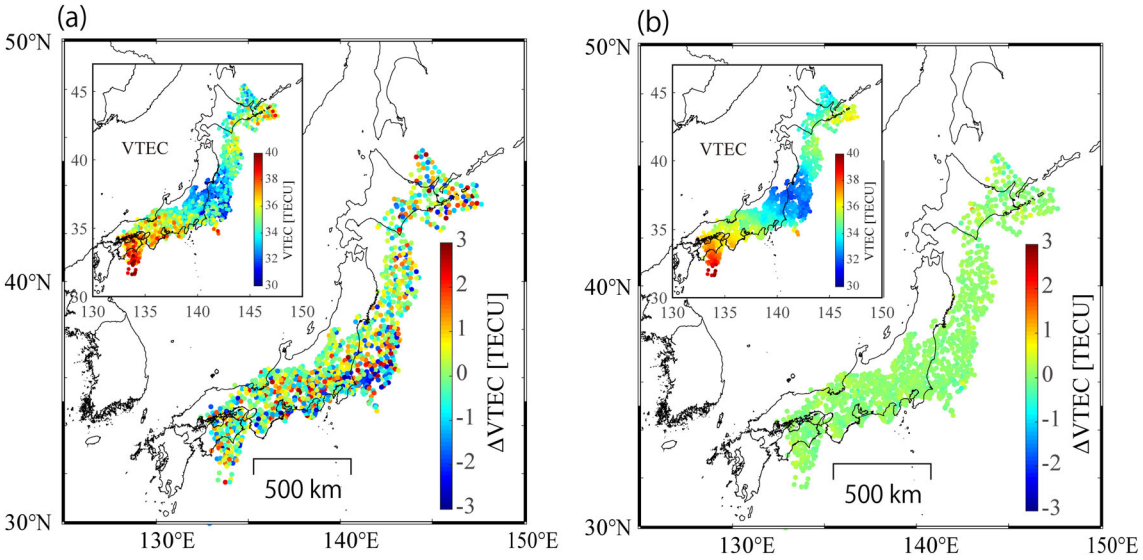

Figure A1. VTEC distribution before and after the correction with PRN15 satellite at 7:20 UT (1 h and 34 min after the mainshock). (a) VTEC residual from the local spatial average before the correction. The dots are color coded to show the VTEC residual value for each IPP location at 300 km height. Imposed panel show the absolute VTEC. (b) Same with Figure A1a but after the correction. The color scales for the main and the imposed panels are common with that in Figure A1a.

correct the ITB to study the faint spatial variation in TEC. We estimate the ITB based on the spatial average of the VTEC every hour. We define $VTEC_{pre\ ij}$ for the ith station and the jth satellite by the weighted average of the measured VTEC as follows:

$$VTEC_{pre\ ij}(t) = \frac{\sum_{m \neq i} VTEC_{mj}(t) \exp\left(-\frac{r_{mi}}{D}\right)}{\sum_{m \neq i} \exp\left(-\frac{r_{mi}}{D}\right)}, \quad (4)$$

where r is the horizontal distance from the SIP to the grid point at location (x, y) and D is the decay distance, which is set to 20 km. The summation is done for the stations within 60 km of the ith station. One ITB is estimated for the trace of each satellite–station pair as the residual between the observed and predicted VTEC:

$$ITB_{ij} = \frac{1}{l} \sum_{n=1}^{l} \frac{\left\{VTEC_{ij}(t_n) - VTEC_{pre\ ij}(t_n)\right\}}{\cos \psi_{ij}(t_n)}, \quad (5)$$

where l is the number of hours in the trace. To deduce the $VTEC_{pre\ ij}$, we select the stations that possess a residual of less than 3 TECU from $VTEC_{pre\ mj}$ for a robust estimation of $VTEC_{pre\ ij}$. We excluded 06:00 UTC during the ITB estimation to avoid the affect of the CID, which starts around 05:55. Each trace generally continues for 1–5 h. We finally obtain the corrected VTEC time series by subtracting $ITB_{ij} \cos \psi_{ij}(t)$ from the initial VTEC time series.

Data Availability Statement

All GPS data were downloaded from Geospatial Information Authority of Japan (https://terras.gsi.go.jp/).

Acknowledgments
We acknowledge Dr. T. Sakai at the Electronic Navigation Research Institute (https://www.enri.go.jp/) and the Astronomical Institute, University of Bern (https://www.aiub.unibe.ch/), for providing the receiver IFBs and satellite DCBs, respectively. We thank K. Heki, M. Kamogawa, and an anonymous reviewer for their critical and constructive comments.

References

Astafyeva, E., Lognonne, P., & Rolland, L. (2011). First ionospheric images of the seismic fault slip on the example of the Tohoku-oki earthquake. *Geophysical Research Letters*, *38*, L22104. https://doi.org/10.1029/2011GL049623

Astafyeva, E., Shalimov, S., Olshanskaya, E., & Lognonné, P. (2013). Ionospheric response to earthquakes of different magnitudes: Larger quakes perturb the ionosphere stronger and longer. *Geophysical Research Letters*, *40*, 1675–1681. https://doi.org/10.1002/grl.50398

He, L., & Heki, K. (2016). Three-dimensional distribution of ionospheric anomalies prior to three large earthquakes in Chile. *Geophysical Research Letters*, *43*, 7287–7293. https://doi.org/10.1002/2016GL069863

He, L., & Heki, K. (2017). Ionospheric anomalies immediately before M_w 7.0–8.0 earthquakes. *Journal of Geophysical Research: Space Physics*, *122*, 8659–8678. https://doi.org/10.1002/2017JA024012

He, L., & Heki, K. (2018). Three-dimensional tomography of ionospheric anomalies immediately before the 2015 Illapel earthquake, central Chile. *Journal of Geophysical Research: Space Physics*, *123*, 4015–4025. https://doi.org/10.1029/2017JA024871

Heki, K. (2011). Ionospheric electron enhancement preceding the 2011 Tohoku-Oki earthquake. *Geophysical Research Letters*, *38*, L17312. https://doi.org/10.1029/2011GL047908

Heki, K., & Enomoto, Y. (2013). Preseismic ionospheric electron enhancements revisited. *Journal of Geophysical Research: Space Physics*, *118*, 6618–6626. https://doi.org/10.1002/jgra.50578

Heki, K., & Enomoto, Y. (2015). M_w dependence of pre-seismic ionospheric electron enhancements. *Journal of Geophysical Research: Space Physics*, *120*, 7006–7020. https://doi.org/10.1002/2015JA021353

Ikuta, R., Satomura, M., Shimada, S., Fujita, A., & Ando, M. (2012). A small persistent locked area associated with the 2011 Mw9.0 Tohoku-Oki earthquake, deduced from GPS data. *Journal of Geophysical Research*, *117*, B11408. https://doi.org/10.1029/2012JB009335

Kakinami, Y., Kamogawa, M., Tanioka, Y., Watanabe, S., Gusman, A. R., Liu, J.-Y., et al. (2012). Tsunamigenic ionospheric hole. *Geophysical Research Letters*, *39*, L00G27. https://doi.org/10.1029/2011GL050159

Kamogawa, M., & Kakinami, Y. (2013). Is an ionospheric electron enhancement preceding the 2011 Tohoku-oki earthquake a precursor? *Journal of Geophysical Research: Space Physics*, *118*, 1–4. https://doi.org/10.1002/jgra.50118

Kamogawa, M., Orihara, Y., Tsurudome, C., Tomida, Y., Kanaya, T., Ikeda, D., et al. (2016). A possible space-based tsunami early warning system using observations of the tsunami ionospheric hole. *Scientific Reports*, *6*(1), 1–7. https://doi.org/10.1038/srep37989

Masci, F., Thomas, J. N., Villani, F., Secan, J. A., & Rivera, N. (2015). On the onset of ionospheric precursors 40 min before strong earthquakes. *Journal of Geophysical Research: Space Physics*, *120*, 1383–1393. https://doi.org/10.1002/2014JA020822

Saito, A., Tsugawa, T., Otsuka, Y., Nishioka, M., Iyemori, T., Matsumura, M., et al. (2011). Acoustic resonance and plasma depletion detected by GPS total electron content observation after the 2011 off the Pacific coast of Tohoku earthquake. *Earth, Planets and Space*, *63*, 863–867. https://doi.org/10.5047/eps.2011.06.034

Sakai, T. (2005). Bias error calibration for observing ionosphere by GPS network. *IEICE Transactions on Communications*, *J88-B*, 2382–2389. (in Japanese)

Shinagawa, H., Tsugawa, T., Matsumura, M., Iyemori, T., Saito, A., Maruyama, T., et al. (2013). Two-dimensional simulation of ionospheric variations in the vicinity of the epicenter of the Tohoku-oki earthquake on 11 March 2011. *Geophysical Research Letters*, *40*, 5009–5013. https://doi.org/10.1002/2013GL057627

Tsugawa, T., Saito, A., Otsuka, Y., Nishioka, M., Maruyama, T., Kato, H., et al. (2011). Ionospheric disturbances detected by GPS total electron content observation after the 2011 off the Pacific coast of Tohoku earthquake. *Earth, Planets and Space*, *63*, 875–879. https://doi.org/10.5047/eps.2011.06.035